Robustness Analysis of Long-Horizon Direct Model Predictive Control: Induction Motor Drives

Ludovico Ortombina
Dep. of Industrial Engineering
University of Padova
Padova, Italy
ludovico.ortombina@unipd.it

Petros Karamanakos
Fac. of Informat. Techn. and Commun. Sciences
Tampere University
Tampere, Finland
p.karamanakos@ieee.org

Mauro Zigliotto
Dep. of Management and Engineering
University of Padova
Padova, Italy
mauro.zigliotto@unipd.it

***Abstract*—Model predictive control (MPC) requires an accurate system model to achieve favorable performance. Thus, in presence of disturbances, model uncertainties and mismatches, MPC needs tools that provide high degree of robustness to them. Since MPC is, essentially, a proportional control technique, an effective method to deal with the aforementioned issues is the addition of an integrating element to the control scheme. This paper presents a prediction model that introduces an integrator to the control strategy without increasing the size of the optimization problem. To examine its effectiveness, the sensitivity of the classical and the proposed MPC to parameter deviations are discussed and analyzed, considering a wide range of switching frequencies as well as prediction horizon lengths. The robustness examination is performed based on an industrial case study, namely a medium voltage induction motor drive.**

***Index Terms*—model predictive control (MPC), induction motor (IM), robustness, parameter sensitivity**

I. Introduction

Over the last decade, direct model predictive control (MPC), also referred to as finite control set MPC (FCS-MPC), has gained much popularity in the power electronic community, not only in academia [1], but also in industry [2], [3]. Some of its numerous advantages include its capability to consider system constraints, to control nonlinear multi-input multi-output, and to fully exploit the available hardware, to name a few.

An inherent disadvantage of MPC is that its performance strongly depends on the accuracy of the system model that serves as the internal prediction model for the optimization problem [4]. Although the power electronic models are typically accurate—at least in comparison with other disciplines, e.g., process control—parameter mismatches are always present in a real-world setup. Hence, such a discrepancy between the actual and the control model can potentially deteriorate the system performance. Moreover, longer horizons, which are usually employed so that MPC can make more educated decisions, and thus improve, e.g., its tracking ability as quantified by the load current total harmonic distortion (THD) [5], are expected to further aggravate the behavior of the controller.

Due to the fact that MPC is a proportional controller [6], i.e., it lacks an integrating element, several techniques have been proposed to address this issue and to curb the associated detrimental effects. Specifically, the proposed techniques mainly adopt one of two different principles, i.e., either to add an integrator to the control strategy to make the MPC structure similar to that of a proportional-integral (PI) controller [7]–[11], or to include a disturbance observer [12]–[14]. The techniques in the latter group consider all parameter mismatches and unmodeled disturbances as exogenous ones. For example, an active disturbance rejection method [12], or a Luenberger observer [13], [14] can be implemented to predict the evolution of the state and/or disturbances and use this knowledge when minimizing the cost function. On the other hand, the integrating element in the former group can be included in different ways, e.g., [10] augments the system state with an additional variable which represents the integrating state. Alternatively, [7], [11] solves the MPC problem by finding the optimal variation of the control action, while the to-be-implemented control input is subsequently computed by integrating the optimal solution. In doing so, the size of the optimization problem remains the same, even though an integrating element is introduced. Finally, in a different direction, [8], [9] modifies the cost function to account for the discrepancy between the reference and measured currents.

To further enhance the robustness of the control scheme to parameter mismatches, the drive model can be adjusted in real time by estimating and tracking the motor parameters variations [15], [16]. Similarly, a gray box approach can be implemented where the motor behavior is described by means of an equivalent model that relies on the free and forced response of motor currents and its coefficients are continuously updated based on the acquired measurements [17].

Before implementing any of the aforementioned methods, however, understanding of the effect of the parameter mismatches on the MPC performance is required. Alas, often the relevant analysis is not conclusive. For example, [14] assesses the control behavior in presence of mismatches in a subset of the drive parameters, namely the rotor and stator resistances and the mutual inductance, whereas the rotor and stator leakage inductances are neglected. Similarly, [18] shows that the controller robustness is susceptible to changes in the load current and the system inductance. Regarding the latter, the controller performance is mostly deteriorated with an overestimated inductance, whereas an underestimated inductance

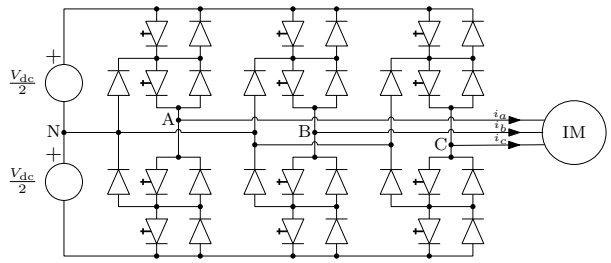

Fig. 1: Three-level NPC voltage source inverter with a induction motor (IM). The inverter has a fixed neutral point potential.

does not adversely affect the system behavior. Hence, for more meaningful conclusions the robustness analysis needs to take into account the combined effect of parameters mismatches. This is more relevant when induction motor (IM) drives are of concern since four state variables and five parameters are required to fully describe their electrical behavior, meaning that several sources of uncertainty could affect the MPC performance.

Motivated by the above, this paper investigates the effect of parameter mismatches on the performance of FCS–MPC for medium voltage (MV) drives, namely a three-level neutral point clamped (NPC) inverter driving an IM. Two different modeling approaches, one with and one without integrator, are discussed. Subsequently, these models are used by MPC and its behavior is assessed when varying all the motor parameters, i.e., the stator and rotor resistances as well as the leakage and mutual reactances. In doing so, the benefits and limitations of the different models are pinpointed and analyzed.

II. Physical Model of the System

The studied system is an MV variable speed drive system with an IM driven by a three-level NPC voltage source inverter as shown in Fig. 1. For modeling and control simplicity, the dc-link voltage $V_{\rm dc}$ of the inverter is assumed to be constant and the neutral point potential v_N zero.

The derivation of an adequate model of the drive system to serve as prediction model for the MPC algorithm is of fundamental importance. In this paper, the system modeling and its control are done in the $\alpha\beta$ stationary reference frame. To this end, any variable in the three-phase (abc) system, i.e., $\boldsymbol{\xi}_{abc} = [\xi_a \ \xi_b \ \xi_c]^T$, is transformed into a two-dimensional variable $\boldsymbol{\xi}_{\alpha\beta} = [\xi_\alpha \ \xi_\beta]^T$, by performing the operation $\boldsymbol{\xi}_{\alpha\beta} = \mathbf{K}\boldsymbol{\xi}_{abc}$, where $\mathbf{K}$ is the Clarke transformation matrix

$$\mathbf{K} = \frac{2}{3}\begin{bmatrix} 1 & -\frac{1}{2} & -\frac{1}{2} \\ 0 & \frac{\sqrt{3}}{2} & -\frac{\sqrt{3}}{2} \end{bmatrix}. \tag{1}$$

Moreover, all quantities are in per unit (p.u.).

First, the model of the inverter is derived. A three–level inverter produces the phase voltages $-V_{\rm dc}/2$, 0, $V_{\rm dc}/2$, depending on the switch position at the corresponding phase. Let $\boldsymbol{u}_{abc} = [u_a \ u_b \ u_c]^T$ denote the three-phase switch position of the NPC inverter, where $u_x \in \mathcal{U} \triangleq \{-1, 0, 1\}$, with $x \in \{a, b, c\}$ being the single-phase switch position. Depending on $\boldsymbol{u}_{abc}$, the output voltage of a three-level NPC inverter in the three-phase (abc) frame can be written as

$$\boldsymbol{v}_{abc} = [v_a \ v_b \ v_c]^T = \frac{V_{\rm dc}}{2}\boldsymbol{u}_{abc} \tag{2}$$

A. Classical Prediction Model

The output voltage of the inverter $\boldsymbol{v}_{\alpha\beta} = \mathbf{K}\boldsymbol{v}_{abc}$ is applied to the stator of the IM, i.e., $\boldsymbol{v}_{\alpha\beta} = \boldsymbol{v}_{s,\alpha\beta}$, where $\boldsymbol{v}_{s,\alpha\beta}$ is the stator voltage. Assuming the stator current $\boldsymbol{i}_{s,\alpha\beta}$ and the rotor flux $\boldsymbol{\psi}_{r,\alpha\beta}$ as state variables, i.e., $\boldsymbol{x} = [\boldsymbol{i}_{s,\alpha\beta}^T \ \boldsymbol{\psi}_{r,\alpha\beta}^T]^T$, and the stator current as the system output, i.e., $\boldsymbol{y} = \boldsymbol{i}_{s,\alpha\beta}$, the continuous-time state-space model of the drive can be written as

$$\begin{aligned} \frac{\mathrm{d}\boldsymbol{x}(t)}{\mathrm{d}t} &= \mathbf{F}\boldsymbol{x}(t) + \mathbf{G}\boldsymbol{u}_{abc}(t) \\ \boldsymbol{y}(t) &= \mathbf{C}\boldsymbol{x}(t)\,, \end{aligned} \tag{3}$$

where the matrices $\mathbf{F}$ and $\mathbf{G}$ can be found based on the voltage and flux equations of an IM, namely

$$\begin{aligned} \frac{\mathrm{d}\boldsymbol{i}_{s,\alpha\beta}}{\mathrm{d}t} &= -\frac{1}{\tau_s}\boldsymbol{i}_{s,\alpha\beta} + \begin{bmatrix} \frac{1}{\tau_r} & \omega_m \\ -\omega_m & \frac{1}{\tau_r} \end{bmatrix}\frac{X_m}{D}\boldsymbol{\psi}_{r,\alpha\beta} + \frac{X_r}{D}\boldsymbol{v}_{s,\alpha\beta}, \\ \frac{\mathrm{d}\boldsymbol{\psi}_{r,\alpha\beta}}{\mathrm{d}t} &= \frac{X_m}{\tau_r}\boldsymbol{i}_{s,\alpha\beta} - \begin{bmatrix} \frac{1}{\tau_r} & \omega_m \\ -\omega_m & \frac{1}{\tau_r} \end{bmatrix}\boldsymbol{\psi}_{r,\alpha\beta} \end{aligned} \tag{4}$$

where $\tau_r = X_r/R_r$, $\tau_s = X_r D/(R_s X_r^2 + R_r X_m^2)$, X_m, $X_r = X_{lr} + X_m$, $X_s = X_{ls} + X_m$, X_{lr}, X_{ls}, R_s, and R_r stand for the rotor and stator time constant, mutual reactance, rotor and stator self reactance, rotor and stator leakage reactance, and stator and rotor resistance, respectively. Moreover, the determinant D is defined as $D = X_s X_r - X_m^2$. Finally, due to the fact that the mechanical dynamics are much slower than the electrical dynamics, the motor speed ω_m is assumed to be constant within a control cycle.

Since MPC is designed in the discrete-time domain, (3) needs to be discretized. To this aim, exact discretization is employed, leading to

$$\begin{aligned} \boldsymbol{x}(k+1) &= \mathbf{A}\boldsymbol{x}(k) + \mathbf{B}\boldsymbol{u}_{abc}(k) \\ \boldsymbol{y}(k) &= \mathbf{C}\boldsymbol{x}(k)\,, \end{aligned} \tag{5}$$

where $\mathbf{A} = \mathbf{e}^{\mathbf{F}T_s}$ and $\mathbf{B} = -\mathbf{F}^{-1}(\mathbf{I} - \mathbf{A})\mathbf{G}$, with $\mathbf{e}$ being the matrix exponential, $\mathbf{I}$ the identity matrix, T_s the sampling interval, and $k \in \mathbb{N}$.

B. Velocity motor model

An alternative motor model can be derived by means of the so-called *velocity form* of the system model [11], [19]. This formulation returns the state and the output variations, i.e., the velocity of these quantities, while the manipulated variable is the control input increment instead of the entire control action which corresponds to the three-phase switch position. According to this, the state, input and output variations, i.e., $\Delta\boldsymbol{x}(k) = \boldsymbol{x}(k) - \boldsymbol{x}(k-1)$, $\Delta\boldsymbol{u}_{abc}(k) = \boldsymbol{u}_{abc}(k) - \boldsymbol{u}_{abc}(k-1)$

and $\Delta \boldsymbol{y}(k) = \boldsymbol{y}(k) - \boldsymbol{y}(k-1)$, are defined. With these, the drive model (5) can be rearranged in its velocity form as

$$\begin{aligned} \Delta \boldsymbol{x}(k+1) &= \boldsymbol{x}(k+1) - \boldsymbol{x}(k) \\ &= \mathbf{A}\Delta \boldsymbol{x}(k) + \mathbf{B}\Delta \boldsymbol{u}_{abc}(k) \\ \Delta \boldsymbol{y}(k) &= \mathbf{C}\Delta \boldsymbol{x}(k). \end{aligned} \tag{6}$$

It is worth mentioning that the system state $\boldsymbol{x}(k)$ in (5) describes the entire stator current and rotor flux vector, whereas $\Delta \boldsymbol{x}(k+1)$ traces only the state difference within the time interval $[k,\, k+1]$. Nevertheless, as can be observed, the velocity formulation (6) resembles the classical formulation (5). This characteristic is exploited in Section IV for adding an integrator to the MPC strategy without increasing the optimization problem size. In doing so, noteworthy rejection capability to exogenous disturbances is achieved [20].

III. Direct Model Predictive Control with Reference Tracking

The aim of the MPC strategy is to find the sequence of control inputs $\mathbf{U}(k) = [\boldsymbol{u}_{abc}^T(k)\ \boldsymbol{u}_{abc}^T(k+1)\ \ldots\ \boldsymbol{u}_{abc}^T(k+N_p-1)]^T$ that best satisfies the control objectives within a horizon of N_p time steps. The control objectives are described by a predetermined performance index, or *cost function*, and the optimal sequence of switch positions, i.e., $\mathbf{U}^*(k) = [\boldsymbol{u}_{abc}^{*T}(k)\ \boldsymbol{u}_{abc}^{*T}(k+1)\ \ldots\ \boldsymbol{u}_{abc}^{*T}(k+N_p-1)]^T$, is that sequence $\mathbf{U}(k)$ that minimizes it. Thus, its definition plays a crucial rule on the overall control performance. Finally, the studied MPC is called direct MPC since it directly chooses the switch positions. This is in contrast to its indirect counterpart which uses a voltage modulator [4].

For the chosen case study, i.e., an MV motor drive, the main objective is the minimization of the stator current tracking error $\boldsymbol{i}_{s,\text{err}} = \boldsymbol{i}_{s,\text{ref}} - \boldsymbol{i}_s$, where $\boldsymbol{i}_{s,\text{ref}}$ is the desired stator current value. This has to be achieved while operating the drive system at low switching frequency. In doing so, the switching power losses can be kept low for an increased converter efficiency. Quantifying these control targets, the following cost function is formulated

$$J(k) = \sum_{\ell=k}^{k+N_p-1} \|\boldsymbol{i}_{s,\text{err}}(\ell+1)\|_2^2 + \lambda_u \|\Delta \boldsymbol{u}_{abc}(\ell)\|_2^2\ , \tag{7}$$

where $\Delta \boldsymbol{u}_{abc}(\ell) \triangleq \boldsymbol{u}_{abc}(\ell) - \boldsymbol{u}_{abc}(\ell-1)$ takes into account the switching transitions involved between two consecutive time steps. Hence, (7) penalizes the evolution of the current error and switching effort over the N_p-step prediction horizon. Note that the scalar $\lambda_u > 0$ is a weighting factor that decides on the trade-off between the current tracking accuracy and the switching effort, i.e., the switching frequency.

With the cost function (7), the optimal sequence of control inputs $\mathbf{U}^*(k)$ is found by solving the following constrained problem in real time

$$\begin{aligned} \mathbf{U}^*(k) = &\arg \underset{\mathbf{U}_k}{\text{minimize}}\ J(k) \\ &\text{subject to (5) or (6)} \\ &\qquad \mathbf{U}_k \in \mathbb{U} \\ &\qquad \|\Delta \boldsymbol{u}_{abc}(l)\|_\infty \leq 1,\ \forall \ell = k, \cdots, k+N_p-1 \end{aligned} \tag{8}$$

where $\mathbb{U} = \mathcal{U} \times \cdots \times \mathcal{U}$ is the $3N_p$-times Cartesian product of the set $\mathcal{U}$ and represents the feasible input set. It is worth noting that the model of the drive system in (8) can be either the classical (5), or the velocity one (6). In the following, the optimal solution with both is reported and discussed. According to the receding horizon policy, once the optimal control sequence $\mathbf{U}^*(k)$ is found, only the first element $\boldsymbol{u}_{abc}^*(k)$ is applied to the converter at the current time-step k, whereas all the remaining elements are discarded. Following, the optimization is repeated at the next time step over a shifted horizon and new measurements and/or estimates.

IV. Integer Least-Squares Problem

The integer optimization problem (8) can be solved efficiently with smart branch-and-bound algorithms, such as the sphere decoding algorithm (SDA) [21], to keep its computational complexity at bay. SDA finds the solution $\mathbf{U}^*(k)$ of (8) as the n-dimensional node, i.e., optimal sequence of switch positions, that has the smallest Euclidean distance from the unconstrained solution $\mathbf{U}_{\text{unc}}(k)$ in a n-dimensional skewed lattice. Equivalently, the optimal solution can be found as the unique sequence of switch positions that lies in the tightest hypersphere of radius ρ centered at the unconstrained solution. Thus, the SDA enables a considerable reduction of the candidate solutions that must be evaluated in real time.

The unconstrained solution $\mathbf{U}_{\text{unc}}(k)$ can be found by relaxing the constraints in problem (8). Moreover, to derive a closed-form expression of $\mathbf{U}_{\text{unc}}(k)$, (8) needs to be written in vector form. To this end, the output reference sequence over the prediction horizon N_p is introduced, i.e., $\mathbf{Y}_{\text{ref}}(k) = \left[\boldsymbol{y}_{\text{ref}}^T(k+1)\ \boldsymbol{y}_{\text{ref}}^T(k+2)\ \ldots\ \boldsymbol{y}_{\text{ref}}^T(k+N_p)\right]^T$. With these, the unconstrained solution $\mathbf{U}_{\text{unc}}(k)$ of (8) for each one of the two discussed prediction models can be found as shown in the following sections.

A. Classical Formulation: Unconstrained Solution

The unconstrained solution of (8) with (5) was derived in [21], i.e.,

$$\mathbf{U}_{\text{unc}}(k) = \mathbf{H}^{-1}\boldsymbol{\Theta}^T(k) \tag{9}$$

where

$$\begin{aligned} \mathbf{H} &= \boldsymbol{\Upsilon}^T\boldsymbol{\Upsilon} + \lambda_u \mathbf{S}^T\mathbf{S} \\ \boldsymbol{\Theta}(k) &= \left(\mathbf{Y}_{\text{ref}}(k) - \boldsymbol{\Gamma}\boldsymbol{x}_{\alpha\beta}(k)\right)^T \boldsymbol{\Upsilon} \\ &\qquad + \lambda_u \left(\mathbf{E}\boldsymbol{u}_{abc}^*(k-1)\right)^T \mathbf{S} \end{aligned} \tag{10}$$

and all matrices are defined in the appendix.

B. Velocity Formulation: Unconstrained Solution

The velocity model (6) resembles the classical one (5) with the difference that instead of the discrete-time instantaneous values of the state and input are replaced by their time increments. Note that the control input $\Delta \boldsymbol{u}_{abc}$ of the velocity model appears as a term in the cost function (7), whereas the velocity model output, i.e., $\Delta \boldsymbol{y}(k+1)$, must be integrated over the prediction horizon to get the entire predicted output current trajectory $\boldsymbol{y}(k+1) = \boldsymbol{y}(k) + \Delta \boldsymbol{y}(k+1)$. By defining the increment of output and input sequences over the prediction horizon, namely $\Delta \mathbf{Y}(k+1) = \left[\Delta \boldsymbol{y}(k+1)^T \ \dots \ \Delta \boldsymbol{y}(k+N_p)^T\right]^T$ and $\Delta \mathbf{U}(k) = \left[\Delta \boldsymbol{u}_{abc}(k)^T \ \dots \ \Delta \boldsymbol{u}_{abc}(k+N_p-1)^T\right]^T$, it follows that

$$\Delta \mathbf{Y}(k+1) = \boldsymbol{\Gamma} \Delta \boldsymbol{x}_{\alpha\beta}(k) + \boldsymbol{\Upsilon} \Delta \mathbf{U}(k)\,. \tag{11}$$

With (11), the complete predicted output current trajectory $\mathbf{Y}(k)$ in vector form can be computed by integrating $\Delta \mathbf{Y}(k+1)$ starting from $\boldsymbol{y}(k)$, i.e.,

$$\begin{aligned}\mathbf{Y}(k) &= \begin{bmatrix} \boldsymbol{y}(k) \\ \vdots \\ \boldsymbol{y}(k) \end{bmatrix} + \begin{bmatrix} \mathbf{I} & \mathbf{0} & \cdots & \mathbf{0} \\ \mathbf{I} & \mathbf{I} & \cdots & \mathbf{0} \\ \vdots & \vdots & & \vdots \\ \mathbf{I} & \mathbf{I} & \cdots & \mathbf{I} \end{bmatrix} \Delta \mathbf{Y}(k+1) \\ &= \widetilde{\mathbf{Y}}(k) + \mathbf{S}_i \Delta \mathbf{Y}(k+1)\,,\end{aligned} \tag{12}$$

which allows to write the cost function (7) in vector form as

$$J(k) = (\mathbf{Y}_{\text{ref}}(k) - \mathbf{Y}(k))^T (\mathbf{Y}_{\text{ref}}(k) - \mathbf{Y}(k)) + \lambda_u \Delta \mathbf{U}^T \Delta \mathbf{U}. \tag{13}$$

Following, by relaxing the feasible set from $\mathbb{U}$ to $\mathbb{R}^{3N_p}$, the unconstrained solution of problem (8) with the new cost function (13) is

$$\Delta \mathbf{U}_{\text{unc}}(k) = \mathbf{H}_i^{-1} \boldsymbol{\Theta}_i^T(k) \tag{14}$$

where

$$\begin{aligned}\mathbf{H}_i &= \boldsymbol{\Upsilon}^T \mathbf{S}_i^T \mathbf{S}_i \boldsymbol{\Upsilon} + \lambda_u \mathbf{I} \\ \boldsymbol{\Theta}_i(k) &= \left(\mathbf{Y}_{\text{ref}}(k) - \widetilde{\mathbf{Y}}(k) - \mathbf{S}_i \boldsymbol{\Gamma} \Delta \boldsymbol{i}_{\alpha\beta}(k)\right)^T \mathbf{S}_i \boldsymbol{\Gamma}.\end{aligned} \tag{15}$$

The unconstrained solution (14) differs from (9) since only the optimal input variation is returned instead of the control action itself. However, unconstrained solutions (9) and (14) have the same complexity since the matrices have the same dimensions. This implies that an integrator term can be added to the MPC strategy without increasing the state vector as opposed in, e.g., [10], [22]. In these works the dimension of the model is increased, making the MPC problem more complex, especially when a long horizon is adopted for improved system performance.

To compute the entire unconstrained solution $\mathbf{U}_{\text{unc}}(k)$, (14) must be integrated from the last applied switch position $\boldsymbol{u}_{abc}(k-1)$, i.e.,

$$\mathbf{U}_{\text{unc}}(k) = \widetilde{\mathbf{U}}(k) + \mathbf{S}_i \Delta \mathbf{U}_{\text{unc}}(k) \tag{16}$$

where $\widetilde{\mathbf{U}}(k) = \left[\boldsymbol{u}_{abc}^T(k-1) \ \dots \ \boldsymbol{u}_{abc}^T(k-1)\right]^T$. In doing so, an integrator is included into the control scheme, thus differentiating the velocity formulation from the classical one. It should be mentioned, however, that the velocity formulation is equivalent to the classical one when no parameters discrepancies exist.

With the unconstrained solution $\mathbf{U}_{\text{unc}}(k)$, the integer solution $\mathbf{U}^*(k)$ of problem (8) can be found by solving

$$\begin{aligned}&\mathbf{U}^*(k) = \arg \underset{\mathbf{U}_k}{\text{minimize}} \ \left\|\bar{\mathbf{U}}_{\text{unc}} - \mathbf{V}\mathbf{U}(k)\right\|_2^2 \\ &\text{subject to } \mathbf{U}_k \in \mathbb{U} \\ &\qquad \left\|\Delta \boldsymbol{u}_{abc}(l)\right\|_\infty \leq 1,\, \forall \ell = k, \cdots, k+N_p-1\,,\end{aligned} \tag{17}$$

where it holds that $\mathbf{V}^T\mathbf{V} = \mathbf{H}$ with $\mathbf{V}$—known as lattice generator matrix—being a nonsingular lower triangular matrix provided that $\lambda_u > 0$. Moreover, $\bar{\mathbf{U}}_{\text{unc}} = \mathbf{V}\mathbf{U}_{\text{unc}}$. Note that regardless of the unconstrained solution $\mathbf{U}_{\text{unc}}$ used, i.e., either in the form (9), or (16), matrix $\mathbf{V}$ is obtained using matrix $\mathbf{H}$ in (10) since it describes the whole system, whereas $\mathbf{H}_i$ models only its increment over time.

To find $\mathbf{U}^*(k)$ with SDA, as mentioned before, the n-dimensional lattice point closest to $\bar{\mathbf{U}}_{\text{unc}}$ needs to be found, i.e., the candidate solution that forms the smallest hypersphere of radius ρ. Hence, to speed up the optimization phase, the initial radius ρ_{ini}, which defines the upper bound of the search process, should be chosen carefully to have a sphere as small as possible from the very beginning of the process. In doing so, the majority of lattice points (i.e., candidate solutions) can be excluded *a priori*. With this in mind, the initial radius can be set as proposed in [23], namely

$$\rho = \min\left\{\rho_a,\, \rho_b\right\},, \tag{18}$$

where

$$\rho_a = \left\|\bar{\mathbf{U}}_{\text{unc}} - \mathbf{V}\mathbf{U}_{\text{bab}}(k)\right\|_2 \tag{19a}$$

$$\rho_b = \left\|\bar{\mathbf{U}}_{\text{unc}} - \mathbf{V}\mathbf{U}_{\text{ed}}(k)\right\|_2. \tag{19b}$$

The radii in (19) are computed based on two different possibilities, namely the so–called Babai estimate $\mathbf{U}_{\text{bab}}$, or the educational guess $\mathbf{U}_{\text{ed}}$. The former corresponds to the rounded unconstrained solution to the closest integer vector, i.e., $\mathbf{U}_{\text{bab}}(k) = \lfloor \mathbf{U}_{\text{unc}}(k) \rceil$, whereas the latter is the previous optimal solution $\mathbf{U}^*(k-1)$ shifted by one time step.

V. Robustness Analysis

The robustness of FCS-MPC to parameter mismatches was examined throughout an extensive set of simulations and is presented hereafter. Specifically, it was studied how the system performance is affected by variations in all motor parameters, namely the rotor and stator resistance as well as the rotor, stator leakage and mutual reactance. To this aim, a mismatch was introduced by varying the value of a parameter in the prediction model, while keeping the same parameter constant in the simulated motor. Moreover, the aforementioned analysis was done for different prediction horizons to investigate the effect of the latter on the system performance. Hence, a $\pm 50\%$ parameter variation and two different prediction horizons,

TABLE I: System nameplate data.

Parameter	Nameplate data	p.u. value
Rated current (I_R)	356 A	
Rated voltage (V_R)	3300 V	
Angular stator frequency (ω_{sR})	$2\pi 50$ rad/s	
Rated speed (ω_R)	596 rpm	
Rated Torque (τ_R)	26.2 kN m	
Pole pairs (p)	5	
Stator resistance (R_s)	57.61 mΩ	0.0108 p.u.
Rotor resistance (R_r)	48.89 mΩ	0.0091 p.u.
Stator leakage reactance (X_{ls})	799 mΩ	0.1493 p.u.
Rotor leakage reactance (X_{lr})	591 mΩ	0.1104 p.u.
Mutual reactance (X_m)	12.57 Ω	2.348 p.u.
Dc-link voltage (V_{dc})	5.2 kV	1.9299 p.u.

namely a one- ($N_p = 1$) and a nine-step ($N_p = 9$) horizon were studied. Moreover, the conventional and the velocity model were compared. Table I lists the parameters of the IM-based motor drive in both absolute and p.u. values. The sampling interval was $T_s = 25\,\mu$s and operation at rated speed and torque was assumed for all simulations. For each of the presented case studies, 300 simulations were carried out with several values of λ_u, i.e., $\lambda_u \in [10^{-3.3}, 10^{-0.5}]$, to achieve operation at a wide range of switching frequencies. Finally, to provide further insight, the product of current THD I_{THD} and switching frequency f_{sw}, i.e., $c_f = I_{\text{THD}} \cdot f_{\text{sw}}$, was employed as a meaningful performance metric [5].

A. Resistance Mismatches

The resistance value can considerably change during the drive operation as a function of the motor temperature. Fig. 2 reports the MPC performance when a stator or a rotor resistance mismatch occurs. Furthermore, for comparison purposes, the nominal motor operation, i.e., without mismatches, is also reported. As can be observed, the stator and rotor resistances have a marginal effect on MPC performance, regardless of the degree of mismatch, or the length prediction horizon. It can be observed that better MPC performance, i.e., a smaller c_f factor, can be achieved with a longer prediction horizon, as also shown in [5]. Both prediction models, i.e., the classic (5) and the velocity one (6), show comparable results. The depicted behavior can be explained from the fact that at full speed and rated motor current, the resistance voltage drop is very small. Hence, any discrepancies in the value of the resistance produce a negligible prediction voltage error that does not affect the overall control performance.

B. Reactance Mismatches

IM can experience magnetic saturation and the values of the machine reactances can vary as the magnetic load changes considerably depending on the operating point. Given that a machine can be assumed as a load with predominantly inductive behavior, and by considering that the MPC performance, as assessed by the metric c_f, depends on the current THD, a simplified motor model is employed to model the impact of harmonics. It consists of the stator resistance, while the

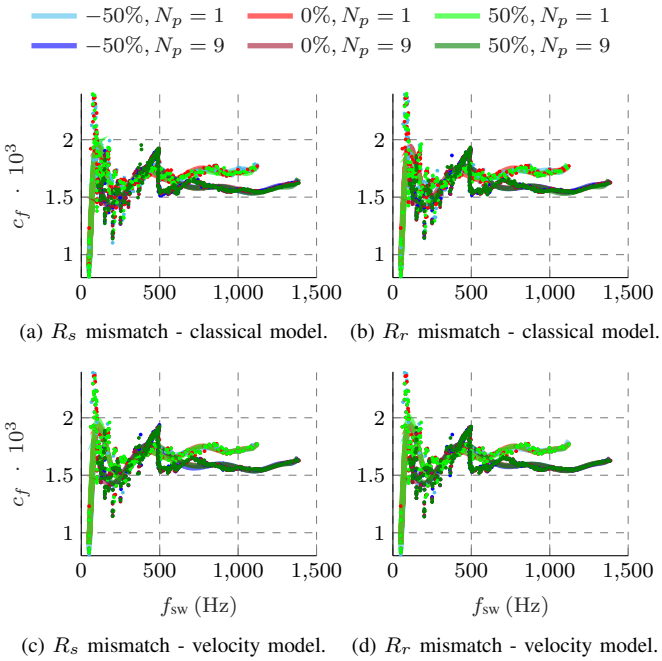

(a) R_s mismatch - classical model. (b) R_r mismatch - classical model.

(c) R_s mismatch - velocity model. (d) R_r mismatch - velocity model.

Fig. 2: Performance metric c_f as a function of the switching frequency f_{sw} when using either the classical, or the velocity model with FCS-MPC and one- ($N_p = 1$) or nine-step ($N_p = 9$) horizon. A $\pm 50\%$ variation in wither the stator R_s or rotor R_r resistance is considered. Metric c_f obtained with nominal system parameters (i.e., no mismatches) is also shown.

motor reactances are modeled by the total leakage reactance $X_\sigma = D/X_r = 0.255$ p.u. Thus, for analyzing the effect of machine reactances mismatches on the system performance, the leakage reactance is varied. To do so, first it is examined how variations in the mutual reactance X_m as well as the stator X_{ls} and rotor X_{lr} self reactances affect X_σ. As can be seen in Fig. 3, a $\pm 50\%$ change in X_{ls}, X_{lr}, or both, causes the biggest variations in X_σ. On the other hand, a mismatch in X_m results in a negligible variation in the leakage reactance, regardless of the degree of mismatch. Hence, a worst control performance, i.e., a bigger c_f, is expected when a discrepancy occurs in the stator or rotor reactance instead of the mutual one. Finally, it is worth noting the asymmetric behavior that characterizes the total leakage reactance sensitivity. For example, a 50% overestimation on X_{ls} and X_{lr} produces a smaller X_σ variation that an underestimation of the same magnitude.

To verify the total leakage reactance approach for estimating the control performance degradation, Figs. 4, 5, and 6 report the performance metric c_f when X_m, X_{lr}, and X_{ls}, respectively, are badly estimated. From the total leakage reactance analysis, it is anticipated for mismatches in the mutual reactance to have marginal detrimental effects on the MPC performance. Such an expectation is confirmed by Fig. 5, where, as can be seen, c_f is almost insensitive to a mutual reactance mismatch, with the velocity model (6) outperforming

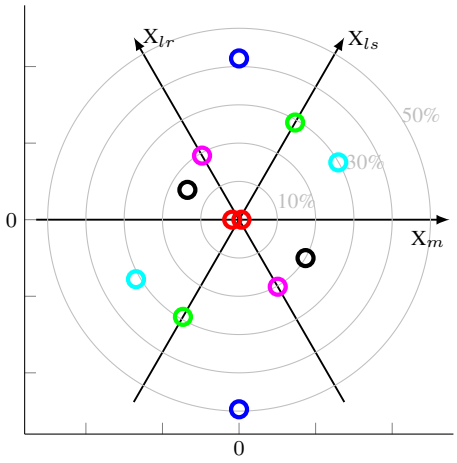

Fig. 3: Change (in %, shown as circles) in the total leakage reactance X_σ for a $\pm 50\%$ variation of X_m, X_{ls}, X_{lr}, or a combination of two. For example, a circle on the positive half of the X_{ls} axis indicates the change in X_σ due to a 50% variation of X_{ls}; a circle between the X_{ls} and X_{lr} axes shows the effect on X_σ when both X_{ls} and X_{lr} are varied, etc.

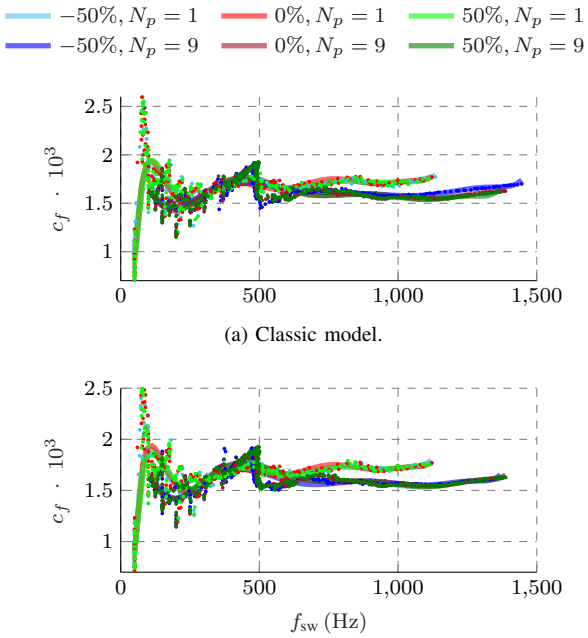

(a) Classic model.

(b) Velocity model.

Fig. 4: Performance metric c_f as a function of the switching frequency f_{sw} when using either the classical, or the velocity model with FCS-MPC and one- ($N_p = 1$) or nine-step ($N_p = 9$) horizon. A $\pm 50\%$ variation in the mutual reactance X_m is considered, i.e., a $\pm 1\%$ variation in the total leakage reactance X_σ. Metric c_f obtained with nominal system parameters (i.e., no mismatches) is also shown.

the classical one (5). Note that the latter leads to a slightly worse performance when X_m is underestimated and a 9-step horizon is implemented.

According to Fig. 3, variations in the rotor and stator leakage reactances affect considerably the total leakage reactance. Indeed a $\pm 50\%$ change in X_{ls} or X_{lr} results in a $\pm 30\%$ or $\pm 20\%$ deviation of X_σ from its nominal value, respectively. Figs. 5a and 6a show the performance of a FCS-MPC based on the classical model (5). As can be observed, the aforementioned mismatches adversely affect the system performance compared to a mutual reactance mismatch, confirming the analysis of Fig. 3. The performance degradation is more pronounced for small values of λ_u, i.e., when the converter switches at high frequencies. This is in line with [24], where it is mentioned that an increased system robustness can be achieved by increasing the weighting factor. On the other hand, a clear trend is not recognized at very low switching frequencies. As for the effect of the horizon length, the MPC performance undergoes an even stronger degradation when N_p = 9, as indicated by the increasing c_f. Finally, it can be observed that an underestimation of the reactance leads to a worse current THD than an overestimation.

The velocity-model-based MPC performance is depicted in Figs. 5b and 6b with an X_{lr} and X_{ls} mismatch, respectively. Comparing the velocity and the classical prediction models for very low switching frequencies ($f_{\text{sw}} \leq 300$ Hz), and regardless of the length of the horizon, MPC with the velocity model achieves (slightly) smaller values of c_f, especially for negative mismatches in X_{lr} or X_{ls} (and thus X_σ). Both models, however, give results very close to those of the nominal case (i.e., model without mismatches), which can be attributed to the receding horizon policy of MPC. Nevertheless, as the horizon increases, the parameter mismatches have a negative impact on the system performance, with the velocity-model-based FCS-MPC underperforming compared to that with the classical one. As can be seen, the former shows a considerable performance degradation, both in terms of the metric c_f and the range of obtained switching frequencies, which increases a lot. The reason for this is that model (6) introduces an integrator that can cause stability issues when λ_u is very small (i.e., at high switching frequencies), as discussed in Section V-C. Such a behavior is in line with the classical control theory, according to which an integrator reduces the phase margin, thus leading the system towards instability. It is worth noting that the most critical condition arises when the reactances are overestimated, as happens with FCS-MPC for permanent magnet synchronous motor (PMSM) drives [20].

C. Stability Analysis

A parameter mismatch can have detrimental effects not only on the system performance, but also on the closed-loop stability. To understand this, some considerations about FCS-MPC are made in the following. FCS-MPC directly applies the three-phase switch position which is chosen among a finite number of candidates, while the applied voltage is limited by the dc-link voltage. This feature, along with the control effort penalization in (7) and the receding horizon policy provide some degree of robustness to model mismatches, thus allowing

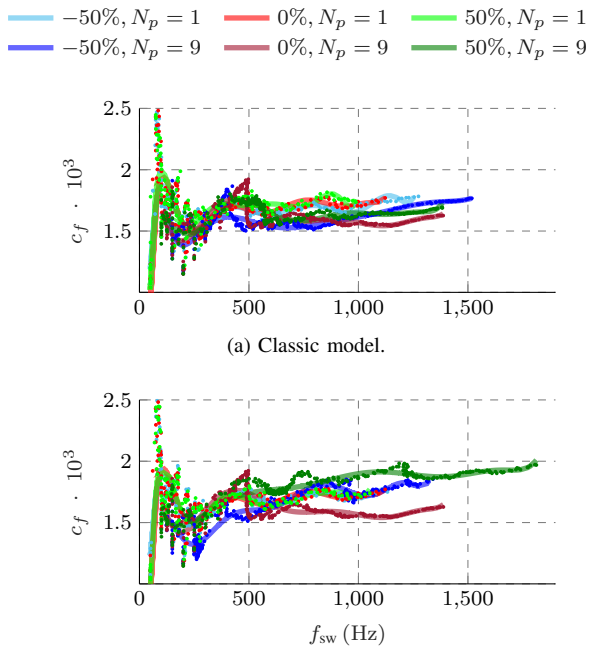

(a) Classic model.

(b) Velocity model.

Fig. 5: The performance metric c_f as a function of the switching frequency f_{sw} when using either the classical, or the velocity model with FCS-MPC and one- ($N_p = 1$) or nine-step ($N_p = 9$) horizon. A $\pm 50\%$ variation in the rotor leakage reactance X_{lr} is considered, i.e., a $\pm 20\%$ variation of the total leakage reactance X_σ. Metric c_f obtained with nominal system parameters (i.e., no mismatches) is also shown.

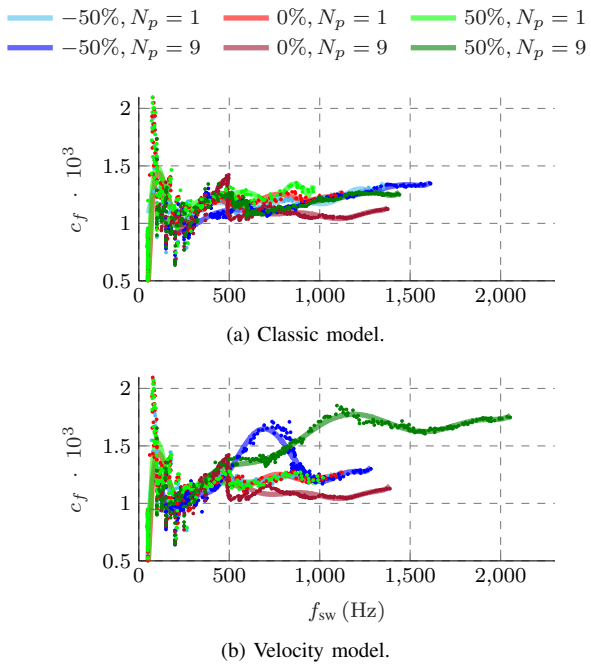

(a) Classic model.

(b) Velocity model.

Fig. 6: The performance metric c_f as a function of the switching frequency f_{sw} when using either the classical, or the velocity model with FCS-MPC and one- ($N_p = 1$) or nine-step ($N_p = 9$) horizon. A $\pm 50\%$ variation in the stator leakage reactance X_{ls} is considered, i.e., a $\pm 30\%$ variation of the total leakage reactance X_σ. Metric c_f obtained with nominal system parameters (i.e., no mismatches) is also shown.

for good reference tracking performance [5]. Despite this, some parameter mismatches deteriorate the tracking quality, as shown in Fig. 5, Fig. 6, and [20].

The stability issue arising with a parameter mismatch can be analyzed with the help of indirect MPC, i.e., MPC with an explicit modulator, which computes the modulating signal which is the same as the unconstrained solution $\mathbf{U}_{\text{unc}}$ for operation in the linear modulation range. Fig. 7 shows the a-component of $\mathbf{U}_{\text{unc}}$, i.e., u_a, and the α-component of $\boldsymbol{i}_{s,\alpha\beta}$, i.e., $i_{s,\alpha}$ within an interval $t = 1\,\text{ms}$ with the classical and the velocity model. Rated speed and current are assumed along with a nine-step prediction horizon and a small weighting factor $\lambda_u = 10^{-5}$. Furthermore, a $\pm 70\%$ mismatch in X_{ls} is considered. As can be seen, the classical model (5) shows a stable behavior with both a positive and a negative mismatch. On the other hand, the velocity model is stable when the stator leakage reactance is underestimated whereas a positive mismatch causes stability issues, as also indicated in Fig. 6. Based on the above, it can be concluded that direct-MPC, i.e., FCS-MPC—if properly designed [5]—can tackle potential stability issues better than its indirect counterpart due to the limited number of switch positions that can be implemented. This, however, comes at a cost of a higher switching frequency, and, thus, power losses.

VI. Conclusion

In this paper the robustness of FCS-MPC to parameter variations of MV IM drive systems was presented. Both positive and negative parameter mismatches were evaluated for all the motor parameters and different prediction horizons. A stator or rotor resistance mismatch has a marginal effect on the MPC performance. The reactance mismatches were studied by using the total leakage reactance of the motor. As shown, the latter is almost insensible to a mutual reactance mismatch, as opposed to mismatches in the stator and rotor leakage reactances. Despite this, the overall MPC performance is slightly affected by the aforementioned mismatches, although a reactance underestimation leads to a slightly higher switching frequency than an overestimated reactance.

In an attempt to enhance the FCS-MPC robustness an alternative prediction model was adopted which relies on the variation of the system state and input. This so-called velocity model includes an integrator into an MPC scheme without augmenting the system state. The subsequent robustness analysis showed that for the meaningful range of switching frequencies for MV drives, i.e., $f_{\text{sw}} \leq 300\,\text{Hz}$, the velocity model provides a better degree of robustness to significant model mismatches. For higher switching frequencies, however, a significant increase in the switching frequency was observed when leakage reactance was overestimated. This was also

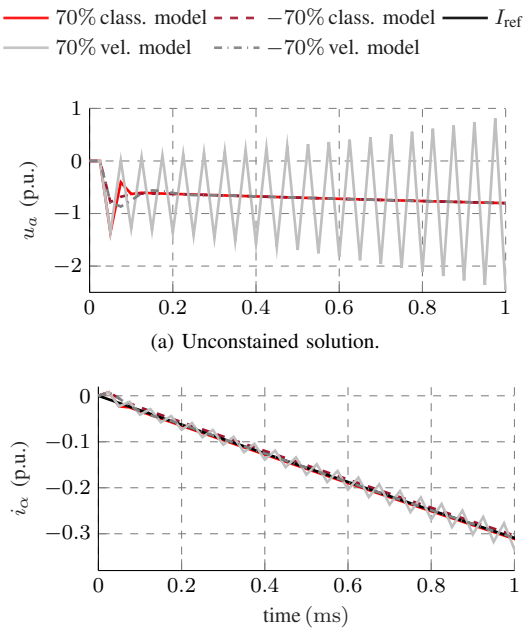

(a) Unconstained solution.

(b) i_α current.

Fig. 7: Unconstrained solution $\mathbf{U}_{\text{unc}}$ and α-component of the stator current when using either the classical, or the velocity model with FCS-MPC, a nine-step horizon and $\lambda_u = 10^{-5}$. A $\pm 70\%$ stator leakage reactance X_{ls} is considered. The current reference is also shown.

verified by the presented stability analysis, according to which FCS-MPC is a robust scheme thanks to its direct control nature and the receding horizon.

APPENDIX

$$\boldsymbol{\Gamma} = \begin{bmatrix} \boldsymbol{CA} \\ \boldsymbol{CA}^2 \\ \vdots \\ \boldsymbol{CA}^{N_p} \end{bmatrix}, \mathbf{S} = \begin{bmatrix} \mathbf{I} & \mathbf{0} & \cdots & \mathbf{0} \\ -\mathbf{I} & \mathbf{I} & \cdots & \mathbf{0} \\ \mathbf{0} & -\mathbf{I} & \cdots & \mathbf{0} \\ \vdots & \vdots & & \vdots \\ \mathbf{0} & \mathbf{0} & \cdots & \mathbf{I} \end{bmatrix},$$

$$\mathbf{E} = \begin{bmatrix} \mathbf{I} \\ \mathbf{0} \\ \mathbf{0} \\ \vdots \\ \mathbf{0} \end{bmatrix}, \boldsymbol{\Upsilon} = \begin{bmatrix} \mathbf{CB} & \cdots & \mathbf{0} & \mathbf{0} \\ \mathbf{CAB} & \cdots & \mathbf{0} & \mathbf{0} \\ \vdots & \ddots & \vdots & \vdots \\ \mathbf{CA}^{N_p-1}\mathbf{B} & \cdots & \mathbf{CAB} & \mathbf{CB} \end{bmatrix}.$$

REFERENCES

[1] P. Cortés, M. P. Kazmierkowski, R. M. Kennel, D. E. Quevedo, and J. Rodríguez, "Predictive control in power electronics and drives," *IEEE Trans. Ind. Electron.*, vol. 55, no. 12, pp. 4312–4324, Dec. 2008.

[2] T. Geyer, N. Oikonomou, G. Papafotiou, and F. D. Kieferndorf, "Model predictive pulse pattern control," *IEEE Trans. Ind. Appl.*, vol. 48, no. 2, pp. 663–676, Mar./Apr. 2012.

[3] T. J. Besselmann, S. Van de moortel, S. Almér, P. Jörg, and H. J. Ferreau, "Model predictive control in the multi-megawatt range," *IEEE Trans. Ind. Electron.*, vol. 63, no. 7, pp. 4641–4648, Jul. 2016.

[4] P. Karamanakos, E. Liegmann, T. Geyer, and R. Kennel, "Model predictive control of power electronic systems: Methods, results, and challenges," *IEEE O. J. Ind. Appl.*, vol. 1, pp. 95–114, 2020.

[5] P. Karamanakos and T. Geyer, "Guidelines for the design of finite control set model predictive controllers," *IEEE Trans. Power Electron.*, vol. 35, no. 7, pp. 7434–7450, Jul. 2020.

[6] A. Bemporad, M. Morari, V. Dua, and E. N. Pistikopoulos, "The explicit linear quadratic regulator for constrained systems," *Automatica*, vol. 38, no. 1, pp. 3–20, Jan. 2002.

[7] A. Favato, P. G. Carlet, F. Toso, and S. Bolognani, "A model predictive control for synchronous motor drive with integral action," in *Proc. IEEE Ind. Electron. Conf.*, Washington, D.C., USA, Oct. 2018, pp. 325–330.

[8] X. Liu, L. Zhou, J. Wang, X. Gao, Z. Li, and Z. Zhang, "Robust predictive current control of permanent-magnet synchronous motors with newly designed cost function," *IEEE Trans. Power Electron.*, vol. 35, no. 10, pp. 10 778–10 788, Oct. 2020.

[9] M. Siami, D. A. Khaburi, A. Abbaszadeh, and J. Rodríguez, "Robustness improvement of predictive current control using prediction error correction for permanent-magnet synchronous machines," *IEEE Trans. Ind. Electron.*, vol. 63, no. 6, pp. 3458–3466, Jun. 2016.

[10] S. Bolognani, S. Bolognani, L. Peretti, and M. Zigliotto, "Design and implementation of model predictive control for electrical motor drives," *IEEE Trans. Ind. Electron.*, vol. 56, no. 6, pp. 1925–1936, Jun. 2009.

[11] G. Betti, M. Farina, and R. Scattolini, "A robust MPC algorithm for offset-free tracking of constant reference signals," *IEEE Trans. Autom. Control*, vol. 58, no. 9, pp. 2394–2400, Sep. 2013.

[12] L. Yan, F. Wang, M. Dou, Z. Zhang, R. Kennel, and J. Rodríguez, "Active disturbance-rejection-based speed control in model predictive control for induction machines," *IEEE Trans. Ind. Electron.*, vol. 67, no. 4, pp. 2574–2584, Apr. 2020.

[13] L. Yan and X. Song, "Design and implementation of luenberger model-based predictive torque control of induction machine for robustness improvement," *IEEE Trans. Power Electron.*, vol. 35, no. 3, pp. 2257–2262, Mar. 2020.

[14] B. Wang, X. Chen, Y. Yu, G. Wang, and D. Xu, "Robust predictive current control with online disturbance estimation for induction machine drives," *IEEE Trans. Power Electron.*, vol. 32, no. 6, pp. 4663–4674, 2017.

[15] S. J. Underwood and I. Husain, "Online parameter estimation and adaptive control of permanent-magnet synchronous machines," *IEEE Trans. Ind. Electron.*, vol. 57, no. 7, pp. 2435–2443, Jul. 2010.

[16] J. L. Zamora and A. Garcia-Cerrada, "Online estimation of the stator parameters in an induction motor using only voltage and current measurements," *IEEE Trans. Ind. Appl.*, vol. 36, no. 3, pp. 805–816, May/Jun. 2000.

[17] F. Tinazzi, P. G. Carlet, S. Bolognani, and M. Zigliotto, "Motor parameter-free predictive current control of synchronous motors by recursive least-square self-commissioning model," *IEEE Trans. Ind. Electron.*, vol. 67, no. 11, pp. 9093–9100, Nov. 2020.

[18] H. A. Young, M. A. Perez, and J. Rodríguez, "Analysis of finite-control-set model predictive current control with model parameter mismatch in a three-phase inverter," *IEEE Trans. Ind. Electron.*, vol. 63, no. 5, pp. 3100–3107, May 2016.

[19] G. Pannocchia and J. B. Rawlings, "The velocity algorithm LQR: a survey," Technical report, University of Wisconsin-Madison, 2001.

[20] L. Ortombina, P. Karamanakos, and M. Zigliotto, "Robustness analysis of long-horizon direct model predictive control: Permanent magnet synchronous motor drives," in *Proc. IEEE Workshop on Control and Model. for Power Electron.*, Aalborg, Denmark, Nov. 2020, pp. 1–8.

[21] T. Geyer and D. E. Quevedo, "Multistep finite control set model predictive control for power electronics," *IEEE Trans. Power Electron.*, vol. 29, no. 12, pp. 6836–6846, Dec. 2014.

[22] F. Stinga and D. Popescu, "Robust model predictive control of an induction motor," in *Proc. Int. Conf. Syst. Theory, Control and Comp.*, Sinaia, Romania, Oct. 2014, pp. 381–386.

[23] P. Karamanakos, T. Geyer, and R. Kennel, "Suboptimal search strategies with bounded computational complexity to solve long-horizon direct model predictive control problems," in *Proc. IEEE Energy Convers. Congr. Expo.*, Montreal, QC, Canada, Sep. 2015, pp. 334–341.

[24] R. P. Aguilera and D. E. Quevedo, "Predictive control of power converters: Designs with guaranteed performance," *IEEE Trans. Ind. Inf.*, vol. 11, no. 1, pp. 53–63, Feb. 2015.